Formation of surface roughness on nanocrystalline aluminum samples under straining by molecular dynamics studies

Aurelien Perron, Olivier Politano, Vincent Vignal

Formation of surface roughness on nanocrystalline aluminum samples under straining by molecular dynamics studies

Journal:	*Philosophical Magazine & Philosophical Magazine Letters*
Manuscript ID:	TPHM-06-May-0137.R2
Journal Selection:	Philosophical Magazine
Date Submitted by the Author:	31-Jul-2006
Complete List of Authors:	PERRON, Aurelien; Universite de Bourgogne, LRRS - UMR 5613 POLITANO, Olivier; Universite de Bourgogne, LRRS - UMR 5613 Vignal, Vincent; Universite de Bourgogne, LRRS - UMR 5613
Keywords:	molecular dynamic simulations, roughness, strain, surfaces
Keywords (user supplied):	

Formation of surface roughness on nanocrystalline aluminum samples under straining by molecular dynamics studies

A. PERRON, O. POLITANO and V. VIGNAL

Laboratoire de Recherches sur la Réactivité des Solides, UMR 5613 - CNRS

Université de Bourgogne, BP 47870, 21078 Dijon, France

Abstract.

The surface roughening of nanocrystalline aluminum samples was investigated by molecular dynamics simulations. Attention was focused on the fact that roughness increases with the grain size and the strain. The elastic-plastic transition was found at around 3.5% strain and a reverse Hall-Petch effect was observed under straining conditions. Then, different strain distributions in grains and grain boundaries at the samples surface was highlighted, yielding to the formation of local roughness. Finally, a linear relationship between the magnitude of roughness and the out-of-plane strain component was found.

1. Introduction.

Surface properties (such as reflectivity, lubricant transport, weldability, adhesion, reactivity in the presence of an aggressive environment, film formation, etc.) play a major role in the processing performance and life cycle assessment of materials (wear, corrosion and environmental degradation, for example). Under straining conditions, surfaces may become rough and surface properties are significantly affected. Therefore, numerous methods including both experimental and modeling studies have been developed in order to measure and predict the surface roughness.

Mahmudi *et al.* [1] have studied the surface roughening during uniaxial and equi-biaxial stretching of 70-30 brass sheets and they found that the roughness increment was proportional to the equivalent strain (between 0 and 0.5) and the grain size (in the range of 18-110 μm). Moreover, Chandrasekaran *et al.* [2] have shown by using atomic force microscopy (AFM) and electron backscatter diffraction (EBSD) that both the surface roughness and the misorientation angle between grains (average grain size of 14 and 60 μm) follow a linear increase with the strain in ultra-law-carbon steel. Other works carried out by Wouters *et al.* [3] on polycrystalline aluminum alloys by means of white light confocal microscopy exhibited a linear relationship between the root-mean-square roughness and both the true strain (between 0 and 0.3) and the grain size (30-90 μm). In addition, Vignal *et al.* have studied the formation of roughness at the surface of stainless steels under straining conditions (applied strain between 0 and 0.045) by using AFM on patterned tensile specimens. They observed that the surface roughness increased with the out-of-plane strain component according to a linear law [4]. They suggest that the surface roughness could be interpreted as a measure of out-of-plane surface displacements. Dispersion in their results might result from

the dependance of the surface roughness on out-of-plane displacements of underlying grains that is not considered in their calculations. By contrast, Mizuno and Mulki [5] found a more complex evolution of the surface roughness of low carbon steel sheets with the strain. In the case of the initial smooth surfaces, roughness grows sharper in the early stages of plastic deformation until a value of 0.3, followed by relatively small increases. Compressive strain causes greater roughening than tensile strain. The initial rough surfaces do not show any remarkable change of roughness in the first stage of deformation until a value of 0.2, and after that they roughen parallel to the smooth surfaces. These previous experiments have shown the dependence of surface roughness on grain size, strain and texture but the relationship between roughness, applied strain and grain size still to be a subject of debate. On the other hand, the experiments of Vignal *et al.* permit to map the microstructural strains at the surface of the patterned tensile specimens by using AFM. The quantification of microstructural strains at the surface of materials is of major importance for understanding the surface reactivity of solids.

Only a few numerical studies deal with formation of roughness according to the strain value, the grain size and orientation. Derlet *et al.* have studied the role played by two parallel free surfaces in the deformation mechanisms of nanocrystalline nickel [6]. However, in most cases, the atomic-scale simulations consider the deformation mechanism of bulk samples in the absence of free surfaces (by introducing periodic boundary conditions). For example, Schiotz *et al.* [7] have investigated the effects of varying temperature, strain rate and porosity on the plastic behaviour of bulk nanocrystalline copper.

The present paper aims at demonstrating the effects of the grain size and the strain value (uniaxial tension) on the formation of roughness at the surface of pure nanocrystalline aluminum samples by means of molecular dynamics simulation (MD). The deformation

mechanisms and the effects of the strain rate were also investigated. The strains distribution at the surface was mapped and compared with surface roughness. Finally, the results obtained from the MD simulation were compared to the experimental approaches.

2. Computational method.

In this paper, we report MD simulations focused on the formation of roughness at the surface of Al samples. Our code is based on the embedded atom method (EAM) with the potential proposed by Ercolessi and Adams [8-9]. This code has already been used successfully to study the multilayer relaxation of Al monocrystalline surfaces under applied deformation [10].

To investigate the formation of surface roughness, we used three different kinds of Al slabs which contained 16 grains with a mean grain size of 5, 10 and 15 nm respectively. In the following, we will refer to these systems by G5, G10 and G15. The polycrystalline samples were created by using a procedure analogous to the one used to obtain Voronoï cells: (1) the centre of the first grain was located at the centre of the three dimensional simulation box with periodic boundary conditions; (2) the 15 other centres were randomly distributed in the simulation box with the condition that two centres must be separated by a distance ranging between 75 and 120% of the grain size fixed initially. For example the grain size lies between 3.75 nm and 6 nm for G5 sample. The 16 grains were built up starting from these seeds. All the grains lattices were disorientated randomly (except for the central one where the (100), (010) and (001) directions coincide with the X, Y and Z direction of the simulation box). Note that all samples have the same microstructure, G10 and G15 samples being a scaled-up

version of the G5. In GBs regions, atoms belonging to different neighbouring grains overlap. In these regions, we removed atoms separated by a distance below 68% of the closest distance in the fcc lattice (i.e. a_0 x $\sqrt{2}/2$ with a_0= 4.05 Å the Al lattice parameter). Considering this criterion, our bulk polycrystalline samples had a density around 97% and no microvoids were observed at the GBs.

The bulk samples were then subjected to an equilibrium procedure, which starts by increasing the temperature, by steps of 50 K from 0 K to 300 K. Changes in temperature were achieved by rescaling the atoms velocities during a 5 ps run (10000 MD steps) using constant number of atoms (N), volume (V) and temperature (T). At each temperature, a 5 ps MD run was also performed by using the Parrinello-Rahman scheme at N, P (pressure) and T constant [11]. The obtained polycrystal at 300K was subsequently relaxed over an extra equilibration run of 10 ps (NVT) steps. This mixing of statistical ensemble was found to be efficient to rapidly obtain a relaxed system at 300K. At this step, free surfaces were created by using the three dimensional simulation box and by placing a slab of vacuum in between the periodic images [12-13]. Practically, this was done by artificially increasing the length of the simulation box along the X-direction (see figure 1(a)). The energy of the system was verified to converge to a stable value. Generally, an increase in the X-direction of 8 nm followed by a NVT run of 10 ps was sufficient to obtain a system with a stable energy. Figure 1(b) shows the microstructure of the G15 slab obtained after relaxation at 300K where the atoms in grey are located in grains (fcc) and those in blue or green at the surfaces or in GBs. The two parallel free surfaces are normal to the X-direction. Then the samples were strained up to +7% along the Y-direction while the length of the box in the Z-direction was maintained constant. Two types of deformation were investigated: (i) a direct deformation where the box and the position of atoms was rescaled instantaneously along the Y-direction in order to obtain the

required strain. The sample was then relaxed during 50 ps (NVT). (ii) a constant strain rate at $5x10^8$ s^{-1}, 10^9 $s^{-1}$and $5x10^9$ s^{-1}. Before analysis, the position of each atom is moved in order to minimize the energy of the system (at V constant) by using a conjugate gradient procedure. The properties of the Al slabs are reported in table 1.

3. Results and discussion.

3.1. Transition between elastic and plastic deformation.

Similar experiments are performed on the G5, G10 and G15 samples. First, the relationships between applied strain, grain size and formation of surface roughness are investigated. The magnitude of the surface roughness is evaluated by measuring the difference between the deepest and the highest atoms of the surface. As shown in table 1, all the unstrained samples have a negligible roughness, suggesting that atoms located at the surface did not move perpendicularly to the surface during the relaxation of the system. Concerning strained samples, we obtained similar amplitude of surface roughness with both types of tensile test (direct and progressive) at 7% strain.

If we consider the computed stress-strain curves given in figure 2 for all systems and strain rates, two different regimes can be observed. The domain below 3.5-4% strain is associated with elastic deformation processes whereas the domain above this limit is related to a plastic regime. Moreover, the slope of each stress-strain curve (i.e. Young's modulus) is calculated in the linear region (elastic regime) for the three samples at $5x10^9$ s^{-1} and it appears that the Young's modulus increases with grain size (52.54, 65.89 and 72.33 GPa for G5, G10

and G15 respectively). Therefore, a clear reverse Hall-Petch effect is observed. This result derived from grain sizes below 20 nm is in agreement with other experimental and numerical works [7, 14, 15]. To investigate the effect of the strain rate, the same system (G10) is strained at $5x10^{8}$ s^{-1}, 10^{9} s^{-1} and $5x10^{9}$ s^{-1}. As exhibited in figure 2, we can observe a strong dependence for strain rates above 10^{9} s^{-1}. In particular, the Young's modulus for the same grain size depends on the strain rate. This last point was studied by Schiotz *et al.* for bulk copper nanocrystalline metals [7]. They have relaxed a sample after strain in the elastic regime and have shown that irreversible strain also occur in this domain (i.e. the system does not regain its initial volume). Below 10^{-9} s^{-1}, the strain rate dependence on the stress-strain curves is less pronounced.

As reported in table 1, an increase of roughness with grain size is observed. This was also observed by Wouters *et al.* [3] who studied surface roughening of polycrystalline Al-Mg alloys during tensile deformation by using white light confocal microscopy. For such systems, they obtained a linear relationship between root-mean-square roughness (rms) and both strain and grain size [3]. In the present work for pure Al, we still observe the same dependence even if our mean grain size is several orders of magnitude lower. However, as shown in figure 3 all strained samples, the roughness increases with strain but does not follow a linear law for all the applied strains. A linear relationship was found between strain and magnitude of roughness below 3.5-4%, which correspond to the elastic regime. Above this value (in the plastic regime), a second linear relationship was observed. The transition between both regimes which is approximately equal to 3.5-4% corroborate the value obtained for the elastic-plastic transition with the stress strain curve (see figure 2).

3.2. Deformation mode.

For grain sizes below 20 nm, there is a competition between two mechanisms of deformation in the plastic domain : an intra-grain mechanism (dislocation) and an inter-grain mechanism (sliding) [16]. We performed a common-neighbour analysis to distinguish atoms located in dislocations (hcp environment), grains (fcc environment) or GBs (other environment) [17, 18]. Figure 4(a) shows the change in the fraction of atoms in different local environments (fcc, hcp and others) for different grain sizes before and after applied strain. As expected the fraction of fcc atoms increases with grain size whereas the fraction of atoms located in the GBs decreases. Moreover, the fraction of fcc atoms decreases and the fraction of atoms located in GBs increases under straining conditions. This shows an expansion of the GBs regions during straining. Note that the fraction of hcp atoms is the same in G5, G10 or G15 samples and slightly increases to reach ~2.5% for a deformation of 7%. To our point of view, even if the increasing number of hcp atoms may be related to dislocation activity, the main deformation is not an intra-grain mechanism but is accommodated in GBs for the studied range of grain size. This is also confirmed by the reverse Hall-Petch effect observed in figure 2.

We have also analyzed more precisely the evolution of the number of hcp atoms during deformation (see figure 4(b)). A noticeable change is also observed at the elastic-plastic transition (3.5-4% strain). Indeed, a sharp increase of hcp atoms is observed in the plastic domain due to the dislocation activity. Note that only a few dislocations emerged at the surface of our samples and their contribution to the formation of roughness was not significant. However, we did not go deeper in the analysis of dislocation activity as this work is focused on the relation between the applied strain and the surface roughness. In particular

and in contrast with others approaches focused on the deformation mechanism in bulk nanocrystalline materials, we did not investigate the character of emitted dislocations [19].

3.3 Surface height distribution.

In our numerical experiments, the roughness is defined as the difference between the deepest and the highest atom of the surface. However, this method is not able to predict if the height distribution is very broad or if this distribution is centred on an average value. Moreover, if the calculated roughness is due only to one atom after deformation, this calculation is not representative of the surface roughness. That is why the surface height distribution is investigated more precisely by dividing the surface into a (21 x 21) mesh for the G5 sample, (41 x 41) mesh for the G10 and (61 x 61) mesh for the G15. Each cell has the same dimension (5 Å x 5 Å and 5 Å x 5.3 Å approximately before and after deformation along Z and Y directions respectively). The height distribution of surfaces is obtained by considering the highest atom of each cell. Using this method, a histogram of the height distribution from average for each sample is obtained (see figures 5(a) and (b) for the G15). It was found that these height distributions follow a Gaussian distribution where the full-width at half-maximum was considered as representative of the surface roughness at the nanoscale. The height distributions from average are narrower for the unstrained samples compared to the strained samples. This confirmed that the unstrained samples have a smooth surface. On the other hand, this last point also shows that the surface roughness calculated by the difference between the deepest and the highest atom of the surface is representative of the entire surface (and not due to a single atom).

These results are qualitatively in agreement with the experimental studies developed by Vignal *et al.* [4]. In these works, electron beam (e-beam) lithography has been used to deposit 16 x 16 arrays of gold-squared pads on a duplex stainless steel with a mean grain size of 50 μm. The diameter of pads was about 300 nm and the distance between centroids of two neighbouring pads was 4 μm. They have determined by AFM the height of each pad before and after 4.5% plastic strain and they have obtained a surface height distribution at the microscale similar to the distribution reported here at the nanoscale (see figures 5(a) and (b)). However, two differences exist between the length scales of analysis. Experimentally, the magnitude of roughness is greater and the height distribution from average is broader. These differences come from the difference in grain size and thus the deformation mode. For the grain size studied experimentally, the main deformation mechanism is related to dislocation activity contrary to our case where no significant dislocation activity is observed. Though some differences are observed between numerical and experimental approaches, the behaviour of the two sets of samples is qualitatively comparable.

Our results can also be compared with the only other existing MD approach on the topic (to our knowledge) [6]. These authors studied the role played by two parallel free surfaces in the deformation mechanism of nanocrystalline nickel by using second-moment tight-binding model of Cleri and Rosato at 300K. Their samples with a grain diameter of 5 or 12 nm were very similar to our systems (see table 1) and they reported a roughness of 3 Å for unstrained surfaces which agree well with the results obtained in the present approach (see sections 3.1 and 3.3). After applying a constant stress, they observed a magnitude of roughness similar to ours (increasing with grain size) and concluded that this behaviour was in part due to increased dislocation activity and also that, for a given small reorientation of an entire grain, there will be a greater movement of atoms for larger grain size. However, in the

present case we were not able to observe the formation of significant steps on the surface due to emerging dislocation and the greater increase in surface roughness in the G15 sample were not clearly related to dislocation activity.

3.4. Mapping of the surface roughness and the strain.

Generally, the surface roughness is studied according to the grain size and the applied strain [1-6]. However to our knowledge there are very few experimental and numerical studies focused on the behaviour of grains and GBs at the surface of the samples. To investigate that point, we map the surface roughness and we compare it with the position of atoms that belong to the grains or to the GBs. The analysis was performed for the three samples and +7% strain. As a similar behaviour was obtained for all samples, we chose to only report the results for the G15 system.

Figure 6 is the mapping of the roughness for the G15 system at +7% strain. The dotted lines correspond to the trace of the GBs at the surface and are only drawn to guide the eyes. With this figure, we clearly observed that bumps at the surface correspond to the grains and hollows to GBs. As shown by this figure, grains and GBs clearly exhibit two different mechanical behaviours and do not behave similarly under straining at the surface of the samples.

We compute the strain at the surface with a mesh similar to the one presented in section (3.3). The stress tensor on an atom is defined as follow [20] :

$$\sigma_i^{\alpha\beta} = \frac{1}{V_i}\left[m_i v_i^{\alpha} v_i^{\beta} + \sum_{\substack{j=1 \\ j\neq i}}^{N} \frac{1}{2} F_{ij}^{\alpha} r_{ij}^{\beta} \right],$$

with α and β the vector components of the vector in Cartesian coordinates, m_i and v_i the mass and velocity of atom i, V_i the atomic volume and F_{ij} the force acting on an atom i due to atom j.

For each cell, which contains approximately 23 atoms, the mean of each atomic strain tensor (σ_{XX}, σ_{YY}, and σ_{ZZ}) is calculated. Figure 7 represents σ_{XX} (perpendicular direction to the surface) for the atoms at the surface after 7% tension (G15). Grains (light grey regions) and the trace of GBs are easily identifiable. Note that σ_{XX} is very different in grains and GBs. Grains undergo a strain close to zero contrary to the GBs which are in tension/compression (up to ±3GPa). As mentioned before, similar results are observed for the G5 and G10 samples. The strain distribution in grains and GBs (figure 7) explained the formation of localized roughness at the samples surface (figure 6).

The surface deformation of the G15 sample after 7% tension was also studied by refining the surface mesh into a 97x97 grid (solid line in figure 8(a)). First, the barycentre of each cell is computed before deformation (the stars in figure 8(a)) and their positions define a perfect square mesh (dotted line in figure 8(a)). Then, the system is deformed and the new positions of the barycentres were calculated (the stars in figure 8(b)). In this case, the barycentres define a deformed mesh as presented in figure 9. From this figure we can clearly distinguish the grains from the GBs where most of the deformation occurred (i.e. in the GBs the initial square mesh is deformed whereas it remains almost perfect in the grains). This also corroborate the inter-grain deformation mechanism observe for our sample (see previous section).

3.5. Deformation and roughness.

The opposite behaviour observed for the grains and GBs under straining conditions explains the formation of roughness in our samples. It was also interesting to map the three-dimensional components of the surface strain field on our sample surfaces and to compare it with experiments on patterned tensile specimens [4]. In these experimental approaches, the in-plane strain components from the average distances was obtained by using the following relationships:

$$\varepsilon_{YY} = \frac{L_Y - L_{Y,0}}{L_{Y,0}}, \qquad \varepsilon_{ZZ} = \frac{L_Z - L_{Z,0}}{L_{Z,0}},$$

where L_Y and L_Z are the average distance between centroids of pads along both the in-plane directions and, $L_{Y,0}$ and $L_{Z,0}$, the average distances before deformation. The out-of-plane strain component was deduced assuming that no changes in volume occur with strain [1, 4]. So the sum of the diagonal terms of the strain tensor is equal to zero:

$$\varepsilon_{XX} = -(\varepsilon_{YY} + \varepsilon_{ZZ}).$$

To compare our results to those reported experimentally, the same relationships were used to compute ε_{XX}, ε_{YY} and ε_{ZZ} even if the hypothesis of volume conservation is not rigorously right for our systems where sample volumes vary between 1.9 to 2.9% before and after deformation (see table 1).

The same technique of 'pads' was used to analyze the simulation results in terms of deformation. The surfaces of the samples (G5, G10 and G15) were divided into a (21x21, 41x41 and 61x61respectively) mesh and the cells were assimilated to the 'pads' used in the experiments. The deformation was obtained by calculating the distance between the barycentres of two cells separated by 3 cells (procedure analogous to figure 8). The spatial period chosen for computational is equal to the gauge length (of about 14 Å). If the cell size is too small (each cell contain a few atoms), the shape of 'pads' change significantly during

deformation and therefore, they can not be used as strain gauge. The problem is the same if the distance between two cells is not enough. This distance defines the number of atoms involved in the calculation of the strain values. Different values of these two parameters have been tried and our calculations converge for mesh division smaller than 97x97 which correspond to cells larger than (3.5 x 3.5) $Å^2$ (above ~9 atoms per cell). We assume that the continuum mechanics of media is valid with these parameters [21]. $L_{Y,0}$ and $L_{Z,0}$ are the distances between two barycentres separated by three cells along the Y and Z direction respectively before deformation (see figure 8(a)). L_Y and L_Z represent the same values after deformation. This leads us to obtain the mapping of the three-dimensional surface strain field (ε_{XX}, ε_{YY} and ε_{ZZ}). Figure 10 represents ε_{XX} at the surface of the G15 sample after 7% traction. The shape of the mapping in figure 10 is very similar to the one reported in the figures 6-7. The grains and the GBs are easily identifiable. As we can notice, ε_{XX} deformation is mainly located in the GBs whereas the centre of the grains is free of deformation.

The average of ε_{XX} and roughness for each grain was then computed. As shown in figure 11 the average surface roughness increased with ε_{XX} according to a linear law. The deviations from the mean value are due to the various orientations but are always in agreement with a linear law. The dispersion of the results might arise from the displacements of underlying grains that are not considered in this calculation of ε_{33}. This linear relationship between ε_{XX} and the roughness was also observed experimentally at the microscale by Vignal *et al.* [4].

4. Concluding remarks.

Molecular dynamics simulations of formation of roughness at the surface of pure Al system under straining conditions were performed. The results were compared with those reported experimentally by Vignal *et al.*. Even if the materials and system sizes studied experimentally and numerically are very different, the results reported by both approaches are qualitatively in good agreement. Moreover, our results agree well with previous MD simulation. The magnitude of the roughness increases with grain size and with strain but the relationship between applied strain and roughness is different in elastic or plastic field. In the present work, the increase of roughness with grain size can not be related to dislocation activity even for the larger system size. Surface height distribution follows a Gaussian distribution before and after deformation. This distribution is broader with increasing strain. The different mechanical behaviour of the grains and the GBs under strain involves formation of roughness. The mapping of the roughness and the strain tensor confirm it. A technique of pads analogous to the one developed for experimental approaches was used to compute surface strains. In addition, the mapping of the diagonal terms of the strain tensor shows that the surface roughness increased with ε_{xx} according to a linear law. In these calculations, the lower distance between two 'pads' corresponds to 14 Å. Below this distance the strain computed with the atomic displacement is not correlable with the imposed macroscopic deformation. In the present approach, the effect of the orientation of the grains and the role played by underlying grains were not investigated. This two points may have a none negligible effect on the formation of roughness under strain and will be studied more extensively in a forthcoming work.

Acknowledgements.

We would like to thank the CRI from the University of Burgundy for allowing us to access their computer facilities. The authors are deeply grateful to D. Kempf and A. Hasnaoui for fruitful discussions.

REFERENCES

[1] R. Mahmudi and M. Mehdiza, J. Mater. Proc. Technol. **80-81** 707 (1998).

[2] D. Chandrasekaran and M. Nygards, Acta Mater. **51** 5375 (2003).

[3] O. Wouters, W.P. Vellinga, R. Van Tijum and J. Th. M. De Hosson, Acta Mater. **53** 4043 (2005).

[4] V. Vignal, E. Finot, R. Oltra, Y. Lacroute, E. Bourillot and A. Dereux, Ultramicroscopy **103** 183 (2005).

[5] T. Mizuno and H. Mulki, Wear **198** 176 (1996).

[6] P. M. Derlet and H. Van Swygenhoven, Phil. Mag. A **82** 1 (2002).

[7] J. Schiotz, T. Vegge, F. D. Di Tolla and K. W. Jacobsen, Phys. Rev. B **60** 11971 (1999).

[8] M.S. Murray, S. Daw and M.I. Baskes, Phys. Rev. B **29** 6443 (1984).

[9] F. Ercolessi and J. B. Adams, Europhys. Lett. **26** 583 (1994).

[10] S. Garruchet, O. Politano, J. M. Salazar and T. Montesin, Surf. Sci. **586** 15 (2005).

[11] M. Parrinello and A. Rahman, Phys. Rev. Lett. **45** 1196 (1980).

[12] Understanding molecular simulation, edited by D. Frenkel and B. Smit, Academic Press, San Diego, 2002, ISBN 0-12-267351-4.

[13] A. Hasnaoui, O. Politano, J.M. Salazar, G. Aral, R.K. Kalia, A. Nakano and P. Vashishta, Surf. Sci. **579** 47 (2005).

[14] A.H. Chokshi, A. Rosen, J. Karch and H. Gleiter, Scr. Metall. **23** 1679 (1989).

[15] T. Yamasaki, P. Schlossmacher, K. Ehrlich and Y. Ogino, Nano-struct. Mater. **10** 375 (1998).

[16] H. Van Swygenhoven, A. Caro and D. Farkas, Mater. Sci. Eng. A **309-310** 440 (2001).

[17] H. Jónsson and H.C. Andersen, Phys. Rev. Lett. 2295 (1988).

[18] A.S. Clarke and H. Jónsson, Phys. Rev. E **47** 3975 (1993).

[19] V. Yamakov, D. Wolf, M. Salazar, S. R. Phillpot and H. Gleiter, Acta Mater. **49** 2713 (2001).

[20] Mesoscopic dynamics of fracture, edited by H. Kitagawa, T. Aihara Jr. and Y. Kawazoe, Springer-Verlag, Berlin, 1998, ISBN 3-540-64291-9.

[21] R. E. Miller and V. B. Shenoy, Nanotechnology **11** 139 (2000).

TABLE CAPTION

Table 1. Characteristics of the Al slabs with a mean grain size of 5 nm (G5), 10 nm (G10) and 15 nm (G15) obtained at 300K with and without applied strain.

FIGURE CAPTIONS

Figure 1. (a) A schematic picture describing the simulation box and the Al samples. The arrows represent the loading directions (L.D.). The box X/Y axes are shown together with relative sizes. The box size along the Z-direction is equal to that along the Y-direction before strain. (b) Microstructure of an Al sample composed by 16 grains with a mean grain size about 15 nm (G15). The atoms in grey are located in grains (fcc) and those in blue or green at the surfaces and in GBs (colored version online).

Figure 2. Evolution of the macroscopic strain tensor (σ_{YY}) versus applied strain (ε_{YY} - L.D.) for G5, G10 and G15 samples at $5x10^9$ s^{-1}. Two other strain rates were tested for the G10 system (10^9 s^{-1} and $5x10^8$ s^{-1}).

Figure 3. Evolution of the roughness versus applied strain (ε_{YY} - L.D.) for G5, G10 and G15 samples.

Figure 4. (a) Fraction of fcc, hcp and other atoms before and after applied strain for G5, G10 and G15 systems. (b) Fraction of hcp atoms during strain ($5x10^8$ s^{-1}) for G5, G10 and G15 samples.

Figure 5. (a) Surface height distribution of G15 system before applied strain. (b) Surface height distribution of G15 system after 7% traction.

Figure 6. Representation of the surface roughness after 7% tension for the G15 system. The dotted lines represent the trace of the GBs and are drawn to guide the eyes.

Figure 7. Representation of the strain tensor (σ_{XX}) at the surface of the G15 sample after 7% tension.

Figure 8. This figure is an enlargement of the G15 surface. (a) The solid lines represent the cells of our mesh (97 x 97) and the stars the barycentres of each cell (the circles correspond to the position of the atoms at the surface). The horizontal arrow ($L_{Y,0}$) is used to calculate ε_{YY} and the vertical arrow ($L_{Z,0}$) to ε_{ZZ}. The squares with bold lines represent the cells assimilated to the 'pads'. (b) Same figure as plotted in (a) but after strain. The stars represent the new positions of the barycentres.

Figure 9. Mesh of the G15 surface after 7% traction. The dotted lines are the trace of the GBs at the surface. A 97 x 97 mesh that correspond to approximately 9 atoms per cell and dimensions cell equal to 3.15 x 3.15 Å is used.

Figure 10. Representation of ε_{XX} at the surface of the G15 sample after 7% traction. The dotted lines are the trace of the the GBs.

Figure 11. Evolution of the surface roughness versus ε_{XX} after 7% traction for the G10 and G15 system.

FIGURE 1

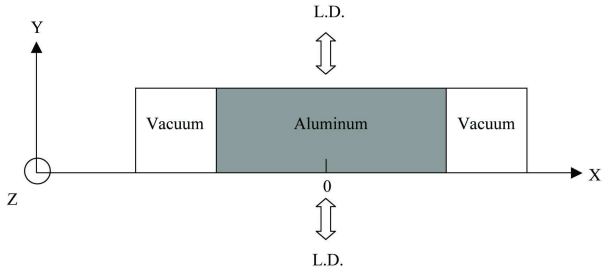

(a)

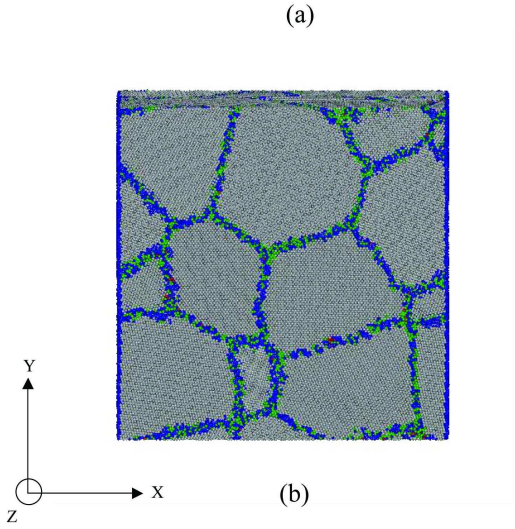

(b)

3

209x297mm (300 x 300 DPI)

FIGURE 2

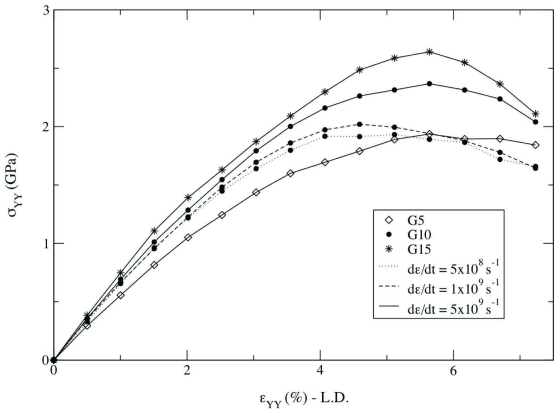

209x297mm (300 x 300 DPI)

FIGURE 3

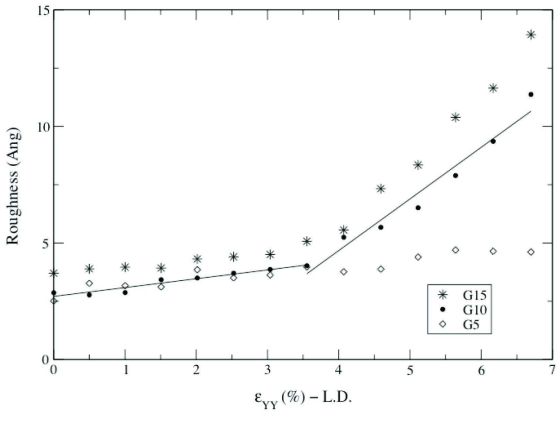

209x297mm (300 x 300 DPI)

FIGURE 4

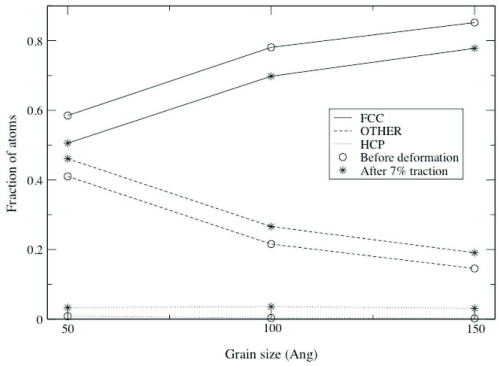

(a)

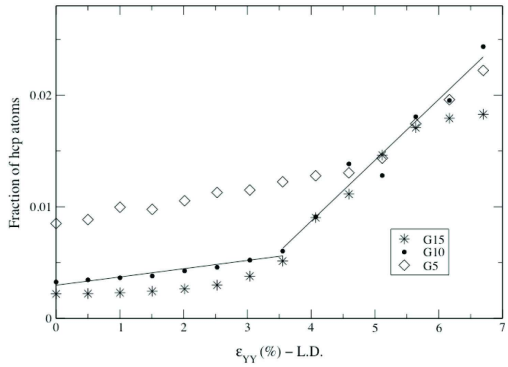

(b)

209x297mm (300 x 300 DPI)

FIGURE 5

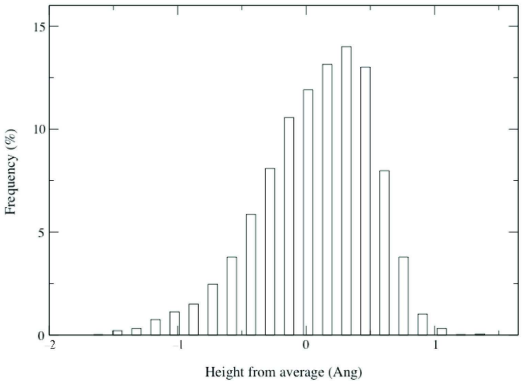

(a)

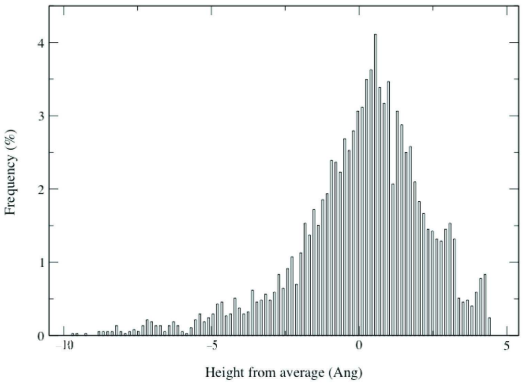

(b)

7

209x297mm (300 x 300 DPI)

FIGURE 6

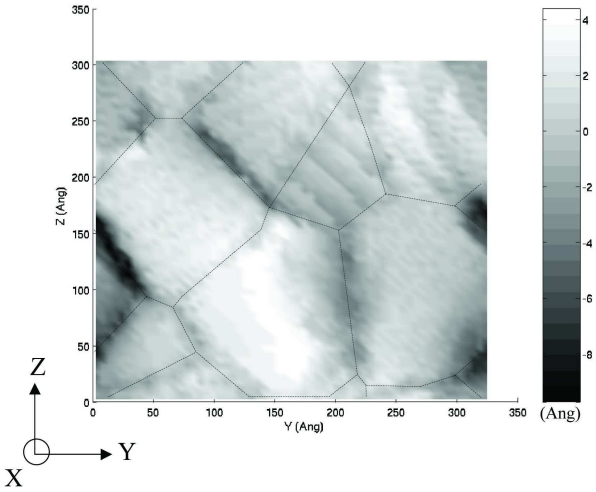

8

209x297mm (300 x 300 DPI)

FIGURE 7

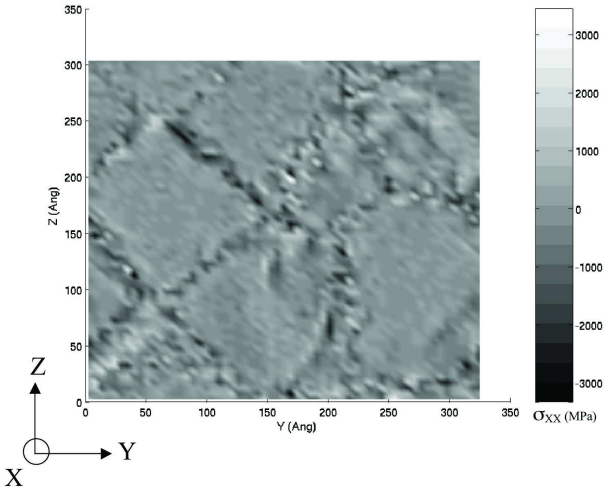

209x297mm (300 x 300 DPI)

FIGURE 8

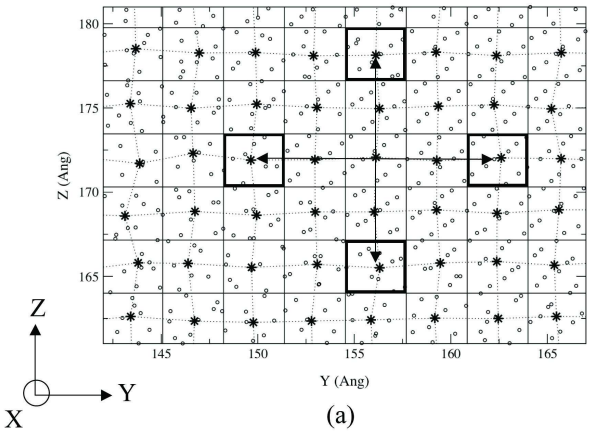

10

209x297mm (300 x 300 DPI)

FIGURE 9

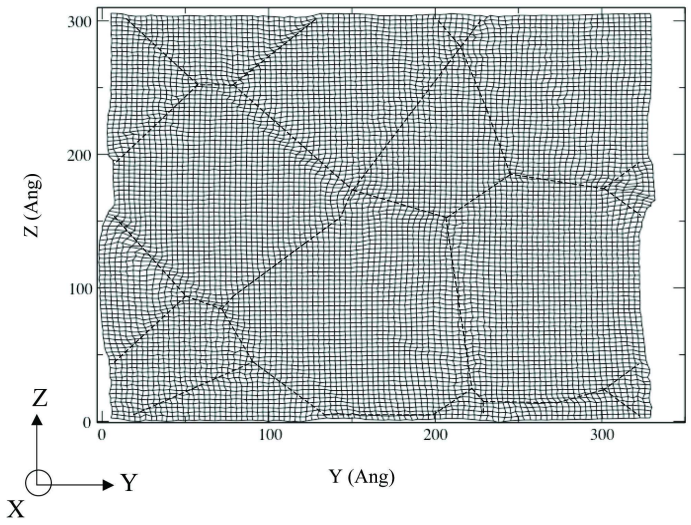

209x297mm (300 x 300 DPI)

FIGURE 10

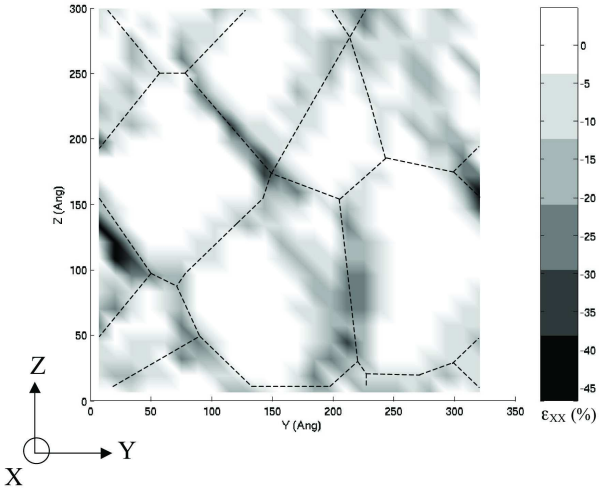

209x297mm (300 x 300 DPI)

FIGURE 11

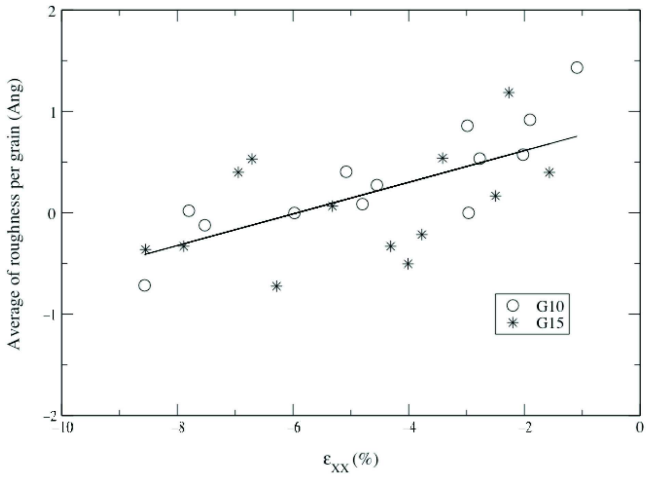

13

209x297mm (300 x 300 DPI)

TABLE 1

Slabs		G5	G10	G15
Number of atoms		62 969	502 871	1 715 645
Unstrained slabs	Volume (nm3)	1 044	8 332	28 440
	Density (%)	98.64	98.75	98.71
	Magnitude of roughness (nm)	0.25	0.29	0.37
Strained slabs (+7%)	Volume (nm3)	1065	8 488	29 262
	Density (%)	95.69	95.97	96.01
	Magnitude of roughness (nm)	0.48	1.15	1.48

209x297mm (300 x 300 DPI)